Journal of Materials Chemistry A

Accepted Manuscript

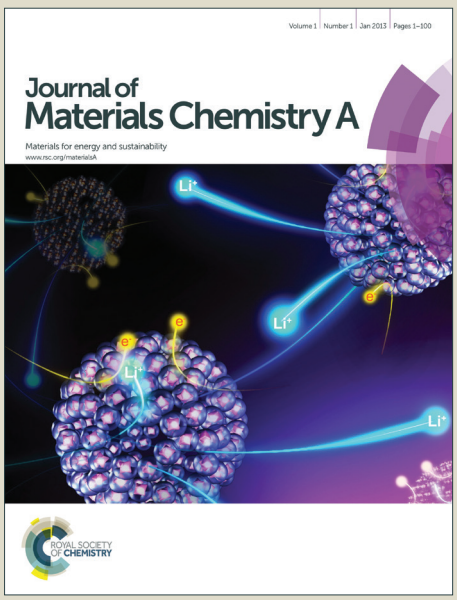

ROYAL SOCIETY OF CHEMISTRY

www.rsc.org/materialsA

Journal of Materials Chemistry A

Cite this: DOI: 10.1039/c0xx00000x

www.rsc.org/xxxxxx

ARTICLE TYPE

A Luminescent Zr-Based Metal-Organic Framework for Sensing/Capture of Nitrobenzene and High-Pressure Separation of CH_4/C_2H_6

Ruyi Zou,[a] Xueling Ren,[d] Fang Huang,[b,d] Yifang Zhao,[c] Jia Liu,[b] Xiping Jing,[c] Fuhui Liao,[c] Yinxia Wang,[c] Jianhua Lin,[c] Ruqiang Zou,[b,*] Junliang Sun [c,*]

Received (in XXX, XXX) Xth XXXXXXXXX 20XX, Accepted Xth XXXXXXXXX 20XX
DOI: 10.1039/b000000x

We present a novel luminescent metal-organic framework (LMOF) based on zirconium metal oxide cluster Zr_6O_8 bonding with a new tetratopic linker 1,3,6,8-tetrakis(4'-carboxy[1,1'-biphenyl]-4-yl-)pyrene. This (4, 12)-connected *ftw-a*-type net is composed of large solvent-accessible 79.5% volume per unit cell with the BET surface area up to 3540.5 $m^2 g^{-1}$. The activated LMOF exhibits unprecedented fluorescence quenching effect triggered by nitrobenzene (NB) with quench percentage up to 99.5%, and could reversibly take up 14.7 mmol g^{-1} of NB under atmosphere condition. The breakthrough curve of CH_4 and C_2H_6 at 298 K and 2.0 MPa demonstates the actived LMOF has high-performance selective adsorption for CH_4 with the selectivity of 25.45, which is an unusually high value as compared with those of reported materials.

Introduction

Metal-organic frameworks (MOFs), a class of porous crystalline materials based on metal ion nodes and organic linkers, have shown excellent performances including but not limited to, gas storage and separation,[1] drug delivery,[2] catalysis,[3] chemical sensors.[4] Among the reported MOFs, a plenty of luminescent MOFs (LMOFs) have been used as the sensors of small molecules,[5a,b] gases,[5c] vapors[5d] and environmental factors such as pH value[7e] and temperature.[5f] The recent several reviews on chemical sensors of LMOFs summarized that the luminescent properties of LMOFs are very sensitive and dependent on various factors.[6-8] Open metal sites of lanthanides or various inorganic clusters and aromatic π-rings or Lewis basic/acidic sites (conjugated p moieties) of various organic linkers can firstly contribute to interactions between the analytes and LMOFs. On the other hand, the solid pore specificity of LMOFs, such as permanent porosity, size, surface and morphology etc., needs to meet the requirement of sensitively and selectively sensing given guest molecules. In addition, some other factors, such as solvent polarity, pH value, temperature, and so on, may play undeniable roles. Thus a wide variety of LMOFs have accurately been constructed and proven successfully in the detection of volatile organic compounds, small molecules, and ionic species, especially nitro aromatic explosive compounds.

Nitrobenzene (NB) is mainly consumed in the production of aniline, which is a precursor to rubber chemicals, pesticides, dyes (particularly azo dyes), explosives, and pharmaceuticals. As a chemical material, it is also used in shoe and floor polishes, leather dressings, paint and organic reaction solvents etc. It is also well-known that NB is highly toxic and carcinogenicity (Threshold Limit Value 5 mg m^{-3}) and readily absorbed through the skin. Therefore the environment and human health issues caused by the use of NB have attracted intensive attention. NB is an electrophilic reagent with a nitro group analogous to many nitro aromatic explosives, so the detection of NB is usually executed along with detection of other nitro explosives. For instance, Li et al. pioneered a LMOF $[Zn_2(bpdc)_2(bpee)]\cdot 2DMF$ (bpdc = 4,4'-biphenyldicarboxylate, bpee = 1,2-bipyridylethene, and DMF = N,N'-dimethylformamide), which could achieve fast and reversible detection of high explosives. The guest-free structure also showed the excellent fluorescence quenching response to NB vapour with the fluorescence quenching percentage of 94% (fluorescence quenching percentage = $(I_o - I)/I_o$ x 100%; I_o = original peak maximum intensity, I = maximum intensity after exposure), which can be attributed to π-π interactions between NB and aromatic π-rings of the host structure and the pore confinement of the analyte inside the molecular-sized cavities.[9] Shi et al. reported a dual functional LMOF $[Zn_3(TDPAT)(H_2O)_3]$ [TDPAT = 2,4,6-tris(3,5-dicarboxylphenylamino)-1,3,5-triazine] as a sensor could quantify the concentration of NB and temperature with excellent linear variation in methanol solution, which due to excellent linear correlation between luminescence intensity and NB concentration/temperature.[10]

To the best of our knowledge, MOFs used as adsorbent materials for NB are seldom reported.[5-8] Here we present a novel Zr-based LMOF with a new tetracarboxylate ligand, H_4TCBPPy (1,3,6,8-tetra(4-carboxybiphenyl))pyrene). This tailored ligand

displays the optically active and strongly fluorescent pyrene core, which is functionalized in the 1-, 3-, 6-, and 8-positions with phenylbenzoate moieties. The target LMOF of $Zr_6O_4(OH)_4(TCBPPy)_3$ (**LMOF-1**) could not only highly-sensitively detect NB together with amazing fluorescence quenching effect but also capture NB in a surprising capacity.

Experimental Section

Synthesis

The solvents and reagents for synthesis were commercially available and used without further treatment. The synthesis and characterization of $H_4TCBPPy$ were summarized in Supporting Information (Scheme S1, Fig. S1-6, Supporting Information). ^1H (^{13}C) NMR and ^1H-^1H COSY measurements were conducted at 40 °C. ^1H NMR (400 MHz, DMSO-d_6) δ (ppm) 12.96 (s, 4H, BiphenylCOO*H*), 8.17 (s, 4H, 4, 5, 9 and 10-Pyrene*H*), 8.05 (d, 8H, J = 8 Hz, 3', and 5'-Biphenyl*H*), 8.00 (s, 2H, 2 and 7-Pyrene*H*), 7.84 (d, 16H, J = 8 Hz, 3, 5, 2' and 6'-Biphenyl*H*), 7.69 (d, 8H, J = 8 Hz, 2, and 6-Biphenyl*H*) (Fig. S4-5, Supporting Information). ^{13}C NMR (100 MHz, DMSO-d_6) δ (ppm) 167.51, 144.17, 140.35, 138.68, 131.59, 130.50, 130.36, 127.99, 127.60, 127.24, 127.10, 126.00, 125.70 (Fig. S6, Supporting Information). In a typical preparation process of **LFMOF-1**, $H_4TCBPPy$ (23.67 mg, 0.024 mmol), $ZrCl_4$ (56 mg, 0.024 mmol) in 10 mL of DMF were ultrasonically dissolved in a 25 mL vial. After the addition of acetic acid (2 mL), the vial was capped and heated at 90 °C for 48 h before being cooled to room temperature slowly. Yellow cubic single crystals were obtained and washed by DMF, Zr (IV)-based yield of 63%. Experimental Details and characterization method are summarized in Supporting Information.

Single-crystal X-ray crystallography

The crystal data was collected on Agilent SuperNava single-crystal X-ray diffractometer at room temperature with Cu-Kα radiation (λ = 1.54 Å). The structures were solved by direct methods using the SHELXS program of the SHELXTL package and refined by full-matrix least-squares methods with SHELXL.[11a] Zr atom in **LMOF-1** was located from the E-maps and other non-hydrogen atoms were located in successive difference Fourier syntheses, which were refined with anisotropic thermal parameters on F_2. The hydrogen atoms of the ligands were generated theoretically onto the specific atoms and refined isotropically with fixed thermal factors. Part solvent molecules in the structure were randomly dispersed, and thus their positions were impossible to refine using conventional discrete-atom models. To resolve these issues, the contribution of solvent electron density was removed by the SQUEEZE routine in PLATON.[11c] Crystal data for **LMOF-1**: cubic, space group *Pm-3m* with a = 24.2929 (4) Å, V = 14336.2 (4) Å^3, Z = 6, ρ_{calcd} = 0.420 g cm^{-3}. Least-squares refinement based on 10984 reflections with I > 2σ(I) and 3067 parameters led to convergence, with a final R_1 = 0.0917, R_{w2} = 0.2731, and GOF = 0.966. CCDC 1062285 contains the supplementary crystallographic data for this paper. These data can be obtained free of charge via www.ccdc.cam.ac.uk/conts/retrieving.html (or from the Cambridge Crystallographic Data Centre, 12 Union Road, Cambridge CB21EZ, UK; fax: (+44) 1223-336-033; or deposit@ccdc.cam.ac.uk).

Powder X-ray diffraction (PXRD)

The PXRD patterns were acquired on a Rigaku Dmax/2400X-ray diffractometer operating at 40 kV and 100 mA, using Cu-Kα radiation (λ = 1.5406 Å).

Thermogravimetric (TG) analysis

TG analysis was carried out under nitrogen atmosphere on a Q600 SDY TGA-DTA-DSC thermal analyzer from room temperature to 800 ˚C with a heating rate of 5 ˚C min^{-1}.

Gas sorption properties

Gas sorption data were collected by a QUANTACHROME AUTOSORB-IQ gas adsorption analyzer. Prior to the sorption measurement, the as-synthesized sample **LMOF-1** was immersed in DMF for around two days, during which DMF was refreshed several times. Then the sample was further dried under vacuum at 100 °C overnight followed by an "outgas" function of the adsorption instrument at 150 °C for 5 h to obtain the activated sample (**LMOF-1a**). **LMOF-1a** still has good crystallinity after the removal of solvent molecules. The N_2 sorption isotherms were acquired in the pressure rage of P/P_0 from 0.01 to 0.99 at 77 K in a liquid nitrogen bath. The gas sorption experiments of CO_2, CH_4, H_2, C_2H_6 and N_2 were conducted at 273 K or 298 K in a glycol-water bath.

Fluorescence measurement

The fluorescence spectra were recorded on a Hitachi F7000 fluorescence spectrophotometer at room temperature. The photomultiplier tube (PMT) voltage was 600 V, the scan speed was 240 nm / min and the slit width of excitation and emission was 2.5 nm. All samples were measured in solid phases. The samples were prepared by introducing 10.0 mg of **LMOF-1a** crystals/powders into 10 mL of DMF, toluene benzene, acetone, ethanol, cyclohexane and NB, respectively, kept in the ultrasonic bath for 5 mins, in air for 3 d standing, then filtered under vacuum to remove the solvents. Similarly, the samples for NB sensing were prepared by introducing 10.0 mg of **LMOF-1a** into 20 mL of cyclohexane with the different content of NB (2, 10, 20, 100, 200 and 1000 μL).

High pressure adsorption

The adsorption equilibrium data were measured on a volumetric setup shown schematically in Scheme S2 (Supporting Information). There are two cells, a reference cell and an adsorption cell. Both cells were kept in a thermostat, whose temperature was 298 K and constant within ±0.1 K. A pressure transmitter model PAA-23/8465.1-200 manufactured by Keller Druckmesstechnik, Switzerland was used to measure its pressure. The deviation from linearity in the whole range of 20 MPa was within 0.05 %.

Experiments were carried out on a setup shown in Scheme S3 (Supporting Information). The fine powder sample (0.183 g) was packed in a tube of length 10 mm and inner diameter 4 mm. Two mass flow controllers (Type SY-9312 of precision ±1 %) were used to control the flow rate of 40 mL min^{-1}. A backpressure regulator was used to control adsorption pressure and a pressure transducer (Type SY-9411 of accuracy ±0.1 %) was used to detect the pressure. The zero point of transducers was adjusted

automatically to compensate for the fluctuation of room temperature.

Composition of the effluent stream was analyzed by a Quadruple mass spectrograph (Stanford Research Systems, Inc. USA) & gas chromatography (GC). All parts were connected by stainless steel capillary tubes of inner diameter 2 mm and wall thickness 0.5 mm.

Results and discussion

Crystal structure description

X-Ray crystallographic analysis indicates that **LMOF-1** crystalizes in a cubic space group *Pm*-3m. The framework consists of the 8-coordinated zirconium oxide cluster Zr_6O_8 linked by tetratopic linkers to form Zr(IV)-carboxylate cluster $Zr_6(\mu_3\text{-}O)_4(\mu_3\text{-}OH)_4(CO_2)_{12}$ as the secondary building unit (SBU) which is similar to that of UiO-66 series (Fig. 1a),[12] but **LMOF-1** was obtained by using tetratopic acid H_4TCBPPy instead of the well-known ditopic acid 1,4-benzenedicarboxylate as the linker.[13] Given the reported Zr-MOF with tetratopic linkers, it is worthy to note that the 12-connected Zr cluster $Zr_6(\mu_3\text{-}O)_4(\mu_3\text{-}OH)_4(CO_2)_{12}$ in MOF-525, 535[14a] and PCN-94,[14b] and $[Zr_8(\mu_4\text{-}O)_6(CO_2)_{12}]^{8+}$ in PCN-221[14c] exhibit the highest O_h symmetry. The 8-c Zr cluster $Zr_6(\mu_3\text{-}O)_8(H_2O)_8(CO_2)_8$ in PCN-222 (MOF545),[14a,d] PCN-521[14e] and NU-1000[14f] shows a higher D_{4h} symmetry, while the 6-c cluster $Zr_6(\mu_3\text{-}OH)_8(OH)_{12}(CO_2)_6$ of PCN-224[14g] with a lower D_{3d} symmetry, and the 8-c cluster $Zr_6(\mu_3\text{-}O)_4(\mu_3\text{-}OH)_4(OH)_4(H_2O)_4(CO_2)_8$ of PCN-225[14h] with the lowest D_{2d} symmetry.

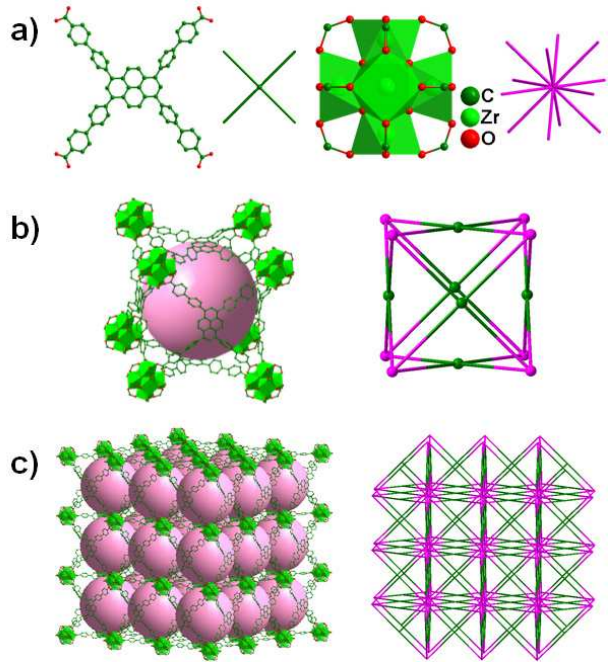

Fig. 1 Crystal structure views of **LMOF-1**: a) the 4-c topological node of TCBPPy and 12-c topological node of Zr_6 cluster, b) cubic cage comprised of Zr_6 clusters and organic linkers and its *ftw-a* topology unit and c) the 3D structure and topological representation of the (4,12)-c network. The space inside cages is highlighted with magenta spheres. All hydrogen atoms and solvent molecules are omitted for clarify.

Obviously the topology of LMOF-1 is analogous to the first type with a ftw-a-type binodal (4,12)-c net and topological point symbol of {436; 630}{44; 62}3. Each TCBPPy moiety connects to four Zr6 clusters (Fig. 1b), and each SBU is bound by twelve carboxylate groups from twelve different TCBPPy moieties (Fig. 1a,c). Such connectivity leads to a three-dimensional (3D) network (Fig. 1c), which features only one type of cubic cages with eight Zr6 clusters occupying the vertices and six TCBPPy moieties covering the faces.

Stabilities

TG analysis of as-synthesized **LMOF-1** displays an obvious decline before 150 °C under N_2 atomphere (Fig. 2), corresponding to the release of solvent molecules incorporated into the pores (64.34% of the total mass). Thereafter the solvent-free framework could be stable up to 500 °C under nitrogen atmosphere, followed by the collapse upon further calcination. The TG curve of the activated sample is no significant weight loss observed before 150 °C because of its effective activation prior to TG, further indicating that the activated sample remains its framework integrity after removal of the guest molecules.

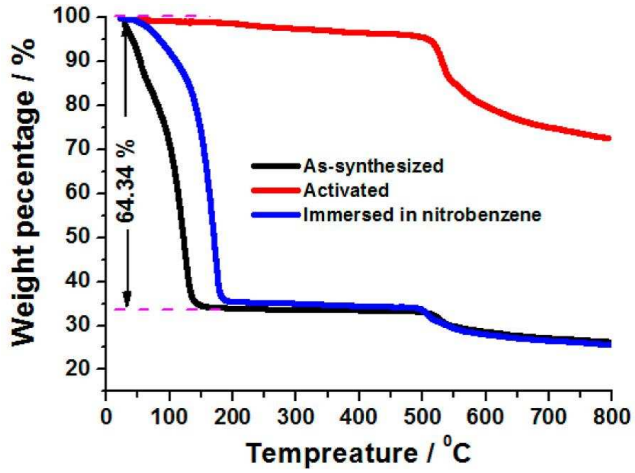

Fig. 2 TGA patterns of **LMOF-1** and **LMOF-1a**, and **NB@LMOF-1a**.

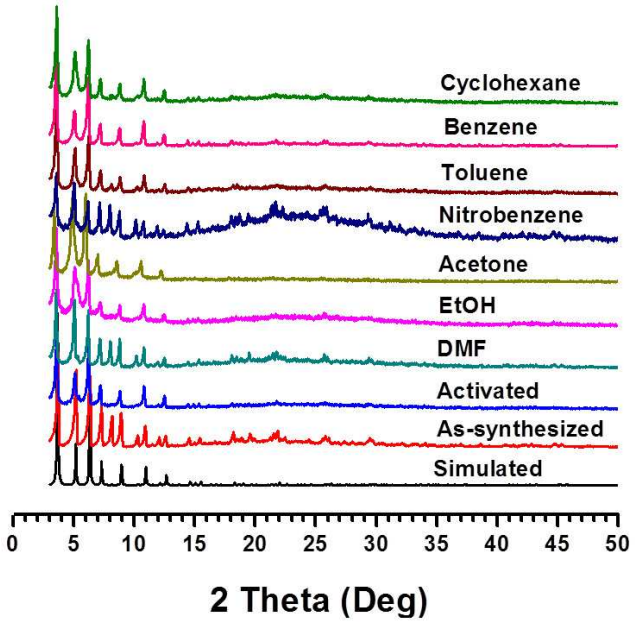

Fig. 3 Comparison of PXRD patterns of **LMOF-1** in different conditions.

The phase purity and stabilities exposed to various organic solvent of bulk **LMOF-1** are investigated by PXRD method. The as-synthesized **LMOF-1** and activiated **LMOF-1a** are in good agreement with the simulated one from crystallographic information file, confirming the phase purity and stability (Fig. 3). **LMOF-1a** was derived from heat treatment of as-synthesized sample at 150 °C for 5 h under high vacuum, which was depended on TG curve of **LMOF-1**. The activated sample also exhibits firmly stability immersed to various solvents, such as cyclohexane, benzene, toluene, nitrobenzene, acetone, ethanol and DMF (Fig. 3 & Fig. S7, Supporting Information).

Porosity

The solvent-accessible volume in **LMOF-1** is 9567.4 Å^3 that constitutes as high as 79.5% volume per unit cell calculated by PLATON routine,[11c] indicating its significantly porous nature. The permanent microporous feature of **LMOF-1a** was experimentally confirmed by gas adsorption measurements (Fig. 4). N_2 adsorption and desorption isotherms at 77 K presented a steep rise at relative low pressure and reached a plateau before 0.2 P_0, which are typical of type-I behavior. The Horvath-Kawazoe (HK) model[15] indicates the pore diameter of 1.41 and 1.71 nm. In terms of the Brunauer-Emmett-Teller (BET) calculation, the surface area was up to 3540.5 m^2 g^{-1}, which is closed to the simulated Connolly surface area 3891.9 m^2 g^{-1} and much higher than that of the ever reported sensing LMOFs that were used to detect nitro explosives.[16]

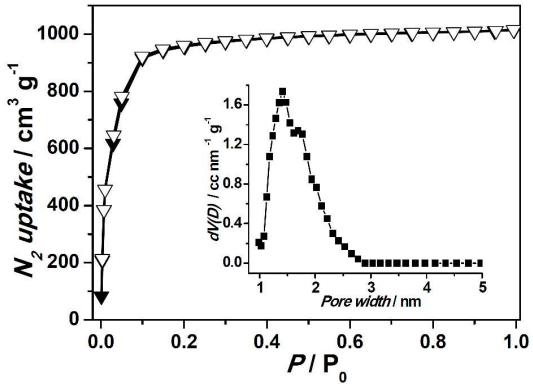

Fig. 4 N_2 adsorption and desorption isotherms at 77 K and pore size distribution (inset) calculated by HK method (Filled shapes: adsorption. Open shapes: desorption).

Fluorescence properties

The solid-state UV-Vis spectrum of free ligand H_4TCBPPy displays a maximum absorption at 370 nm which arises from the π–π* transition of the aromatic rings (Fig. S8, Supporting Information).[17] Then the excitation wavelength of 370 nm was set from the UV/vis spectral data to excite these samples. The solid-state fluorescent emission spectra of H_4TCBPPy and **LMOF-1** exhibited strong emission at 533 and 492 nm, respectively. An obvious blue shift of 41 nm was observed. Based on the similar phenomena,[17] there seems no evidence that the emission spectrum is disturbed by the Zr binding since the shape of their spectra remains the same. This blue shift should be due to decrease of HOMO orbital energy in **LMOF-1** when TCBPPy is firmly fixed in the cubic framework.[18] The fluorescence of **LMOF-1a** displays a strong emission band at 499 nm with a small shoulder at λ_{max} = 447 nm, and a slightly red shift of 7 nm and significant decrease of the emission intensity with respect to as-synthesized **LMOF-1**, which could be related to an amount of strong polar DMF molecules encapsulated in the cages. This solvent effect was confirmed by the solid-state fluorescent spectrum of **LMOF-1a** soaked with DMF (Fig. S9, Supporting Information).

In order to explore the solvent effect on fluorescence properties, the emission spectra of **LMOF-1a** soaked in different solvents were measured, entitled Sol@LMOF-1a (Sol = DMF, Toluene, Benzene, Acetone, Cyclohexane, EtOH or NB; Fig. S9, Supporting Information). It is interesting to note that the linker-centered emission of **LMOF-1** exhibited different solvent-dependent fluorescence phenomena.[19-21] The emission spectra of all samples soaked in different solvents presented disappearance of the shoulder at λ_{max} 447 nm in comparison with that of **LMOF-1a** and different red-shifted degrees compared to that of **LMOF-1**. The emission intensity changes were also correlated with the type of solvent molecules. The fluorescence intensity of the **DMF@LMOF-1a** is almost equal to that of the as-synthesized **LMOF-1**, displaying **LMOF-1** could be reversed to the original structure by reintroducing DMF. The emission spectra of **LMOF-1a** soaked with toluene and benzene exhibited a strong fluorescence enhancement similar to that soaked with DMF, which is due to electron transform from electron-rich toluene and benzene to TCBPPy upon excitation by π-π stacking interactions of the donor-acceptor aromatic rings.[16] Significantly, the sample with NB incorporated demonstrated the strongly quenching and a visible color change from pale yellow to dark yellow with the emission disappeared under UV lamp (365 nm) (Fig. 5a). The fluorescence quench percentage of **NB@LMOF-1a** was up to 99.5 % compared to that of **LMOF-1a** (Fig. 5a), which is, to the best of our knowledge, the highest value among LMOFs detecting nitrocompounds.[9,21] This obvious quenching phenomenon is related to the π-stacking interactions between TCBPPy and NB with significant electron transfer from electron-donating TCBPPy to high electron-deficient NB upon excitation, resulting in the detectable luminescence quenching.[22] In addition, DMF enhanced the emission intensity by 183.4% compared to that of **LMOF-1a**, followed by toluene (178.3%), benzene (166.9%) and Acetone (49.4%), but protonic solvent ethanol had fluorescence quench percentage of 55.9%, followed by aprotic solvent cyclohexane (5%).

Considering the little effcet of cyclohexane as a solvent to the fluorescence intensity of **LMOF-1a**, the samples of **LMOF-1a** soaked in the cyclohexane with the different content of NB were prepared to further examine it sensing sensitivity for NB. As shown in Fig. 5b, the fluorescene intensity of **LMOF-1a** decreased along with the concentration increase of NB in cyclohexane solution. The maximum fluorescence intensity of **LMOF-1a** was decreased by 21.2% upon adding 0.01 vol% (1 x 10^{-3} mol L^{-1}) of NB, and the quenching percentage reached up to 93.5% with respect to NB concentration of 5 vol% (0.5 mol L^{-1}). The sensitivity and outstanding adsorptivity are related to not only host-guess π-stacking interactions and the high surface area described above but also the pore confinement of NB inside the cages of **LMOF-1a**. By using Molecular dynamic simulation, desity distribution of adsorbed NB on **LMOF-1a** was observed clealy (Fig S10, Supporting Informaiton). It is noticed that NB molecules were firstly adsorbed around benzene ring due to the strong π-stacking interactions. With increasing the loading, NB molecules start to be adsorbed around pyrene, which cause

obvious fluorescent quenching behavior of pryrene rings thought the excited electrons transfermation from electron-donating TCBPPy to high electron-deficient NB. This simulation result powerfully supports the experimental data that the quench percentage is linearly to concentration of NB. In terms of the X-ray crystal structure analysis, NB, kinetic diameter *ca.* 5.9 Å,[23] can be incorporated into the cages in **LMOF-1a** because the size of the windows between two neighbouring faces in a cubic cage is more than 1.4 nm (Fig. 4), which was also confirmed by the TG curve in Fig. 2. **NB@LMOF-1a** has a significant mass loss rate of 64.34% within 150 °C to restore to solvent-free **LMOF-1a** again. Notedly, each unit cell can adsorb 53 NB molcules, highlighting that solvent-free **LMOF-1a** can reversibly takes up 14.7 mmol g^{-1} of NB under 298 K and 1 atm, which is obviously higher than that of reported zero-valent iron loaded silica nanoparticles (1155 mg g^{-1}, 9.4 mmol g^{-1})[24a] and the modified activated carbon (1,443.53 mg g^{-1}, 11.7 mmol g^{-1}).[24b] NB vapor can be condensed in the pore at the experiment temperature when the vapor pressure pressurized to it saturated pressure. The LMOF is extremely porous with large pore volume. The NB vapor can be condensed easily in the nano-sized pore based on the capillary condensation mechanism. The condensed NB is full of the pore at the pressure of P/Po=1. The uptakes are linear dependent on the pore volume value. This indicates **LMOF-1a** should be an unprecedented and potential adsorbent material for NB.

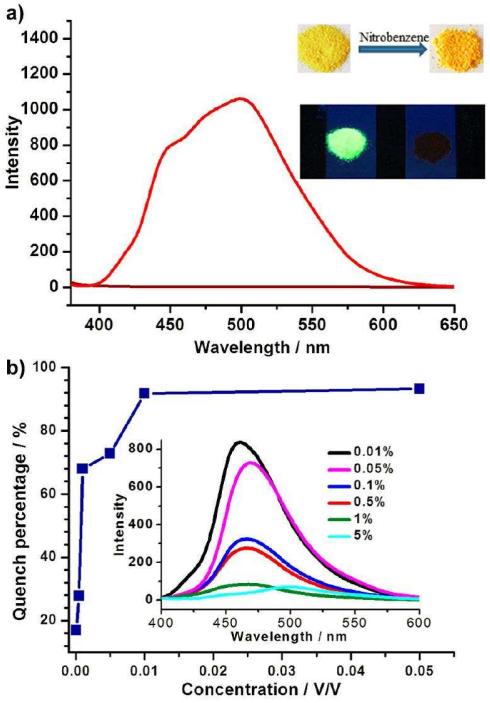

Fig. 5 Solid-state fluorescence emission spectra: (a) **LMOF-1a** (red) and **NB@LMOF-1a** (wine). Insets: photograph of color changes of **LMOF-1a** under the air and UV lamp (365 nm) (Upper), and before and after immersed in NB (Lower); and (b) concentration-dependent fluorescence quench of **LMOF-1a** soaked by cyclohexane with the different content of NB. The inset: the corresponding solid-state fluorescence spectra under λ_{ex} = 370 nm.

Gas sorption and separation properties

MOFs are primitively highlighted by gas sorption and separtion capacity since their high surface area and tunable porosity.[25] Given that **LMOF-1** exhibits high predicted and experimental BET surface areas, CO_2, CH_4, N_2 and C_2H_6 adsorption isotherms were collected at 273 and 298 K, repectively (Fig. 6). **LMOF-1a** takes up 1.93 mmol g^{-1} (43.1 cm^3 g^{-1}) of CO_2 under 273 K and 1 atm, followed by 1.11 mmol g^{-1} (24.8 cm^3 g^{-1}) under 298 K and 1 atm. Because the CO_2 adsorption isotherm of **LMOF-1a** is not fully saturated, a much higher carbon dioxide adsorption capacity (29.91 mmol g^{-1} or 669.8 cm^3 g^{-1}) was collected under 3.8 MPa. Which is far more than that of N_2, H_2 and CH_4 under the same conditions (Fig. 7a).

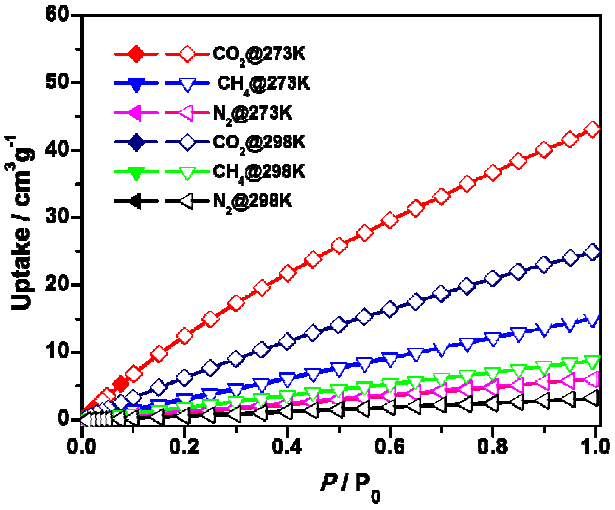

Fig. 6 Gas adsorption isotherms of **LMOF-1a** for CO_2, CH_4 and N_2 at 273 and 298 K (Filled shapes: adsorption. Open shapes: desorption).

It is also worthy to note that **LMOF-1a** takes up much higher amounts of C_2H_6 (21.53 mmol g^{-1} or 482.3 cm^3 g^{-1}) than methane (6.92 mmol g^{-1} or 155.0 cm^3 g^{-1}) at 3.1 MPa and 298 K (Fig. 7a), indicating a promising application of CH_4/C_2H_6 separation. As is well-known, C_2H_6 from natural gas is considered more profitable as feedstocks to produce ethylene for plastics inductry than that from conventional petroleum-derived naphtha routine. Therefore, the separation of C_2H_6 from CH_4 is endowed with the vital significance for not only fundamental science but also industrial applications. Some sorbents have been developed with high selectivity towards C_2H_6 at low pressures,[26] but few of them at high pressures, an economical and effective method to obtain a large amount of C_2H_6. The selective adsorption behavior of **LMOF-1a** toward C_2H_6 and CH_4 was investigated and extended Langmuir equation model was used to calculate the selectivity. The adsorption selectivity of adsorbents was usually reported as the thermodynamically defined:

$$\alpha_{ij} = \frac{(x/y)_i}{(x/y)_j}$$

Here, x and y are the molar fraction of component i and j in the adsorbed and gas phase at equilibrium. The selectivity can be evaluated based on breakthrough curves collected experimentally with gas mixtures. As shown in Table S2 (See Supporting Information), the selective result was calculated by breakthrough curve at condition of 298 K and 2.0 MPa which is simulated the nature environments. The selectivity of 25.45 is a high value among the experimental results that have been reported on any

kinds of materials. To our knowledge, the reported mesoporous carbon [27a] and activated UTSA-36a [27b] exhibit highly selective adsorption of C_2H_6 over CH_4 with selectivity of 19.6 and 16.6 at analogous conditions, respectively, which are much lower than that of this work. It should be attributed to suitable pore size and π-system pyrene moieties of cubic cages in the target LMOF.

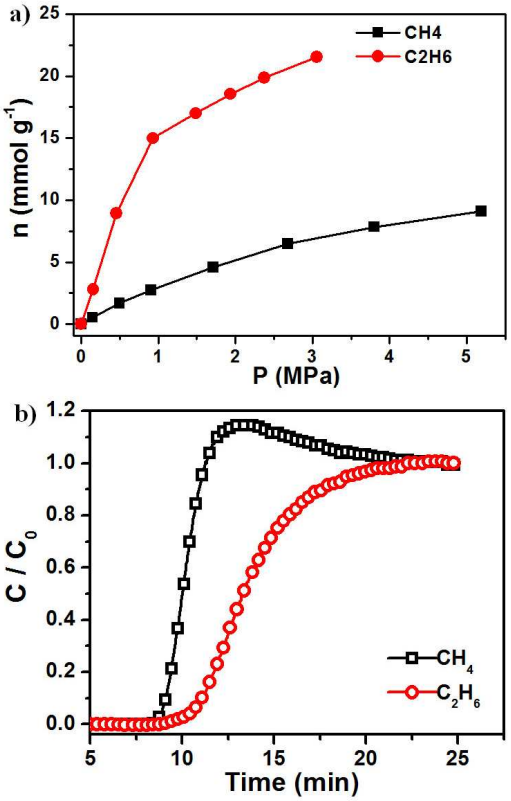

Fig. 7 (a) High-pressure adsorption isotherms of **LMOF-1a** for CH_4 and C_2H_6 at 298 K. (b) breakthrough curve of CH_4 and C_2H_6 at 298 K and 2.0 MPa.

Conclusions

In summary, we have successfully constructed a highly porous *ftw-a*-type LMOF by using a new rigid pyrene-derived tetracarboxylate as linkers. The activated LMOF exhibits high surface area, and efficient fluorescence quenching effect triggered by NB. This work illustrates a rare example that this Zr-LMOF is an unprecedented and potential adsorbent material for NB. In addtion, the breakthrough experiment demonstates that guest-free LMOF is a promising potential for the highly selective separation of C_2H_6 over CH_4.

Acknowledgements

This work was supported by National Natural Science Foundation of China 51322205 and 21371014, New Star Program of Beijing Committee of Science and Technology (2012004).

Notes and References

[a] *College of Chemistry and Molecular Engineering, Zhengzhou University, Zhengzhou 450001, Henan, China*

[b] *Beijing Key Laboratory for Theory and Technology of Advanced Battery materials, Department of Materials Science and Engineering, College of Engineering, Peking University, Beijing 100871, China. Fax: +86-10-62760532; Tel: +86-10-62760532; E-mail: rzou@pku.edu.cn.*

[c] *College of Chemistry and Molecular Engineering, Peking University, Beijing 100871, China. E-mail: junliang.sun@pku.edu.cn.*

[d] *School of Pharmaceutical Sciences, Zhengzhou University, Henan, 450001, China.*

† Electronic Supplementary Information (ESI) available: Synthesis of the ligand H_4TCBPPy (Scheme S1), Crystal structure data (Table S1), Schematic structure of setup for high pressure adsorption and breakthrough curve (Scheme S2, S3), NMR spectra of intermediates and 1,3,6,8-tetra(4-methoxycarbonylbiphenyl)pyrene (Fig. S1-6), PXRD patterns (Fig. S7), Solid-state fluorescence spectra (Fig. S8-9), Adsorptive desity field (Fig. S10). For ESI and catallographic data in CIF or other electronic format see DOI:10.1039/b000000x/.

1. a) M. P. Suh, H. J. Park, T. K. Prasad and D.-W. Lim, *Chem. Rev.*, 2012, **112**, 782-835; b) L. J. Murray, M. Dincă and J. R. Long, *Chem. Soc. Rev.*, 2009, **38**, 1294-1314; c) W. M. Bloch, R. Babarao, M. R. Hill, C. J. Doonan and C. J. Sumby, *J. Am. Chem. Soc.*, 2013, **135**, 10441-10448; d) J.-R. Li, J. Sculley and H.-C. Zhou, *Chem. Rev.*, 2012, **112**, 869-932; e) P. Nugent, Y. Belmabkhout, S. D. Burd, A. J. Cairns, R. Luebke, K. Forrest, T. Pham, S. Ma, B. Space, L. Wojtas, M. Eddaoudi and M. J. Zaworotko, *Nature*, 2013, **495**, 80-84; f) D.-X. Xue, A. J. Cairns, Y. Belmabkhout, L. Wojtas, Y. Liu, M. H. Alkordi and M. Eddaoudi, *J. Am. Chem. Soc.*, 2013, **135**, 7660-7667; g) Z. J. Zhang, W. Y. Gao, L. Wojtas, S. Q. Ma, M. Eddaoudi and M. J. Zaworotko, *Angew. Chem. Int. Ed.*, 2012, **51**, 9330-9334.

2. a) P. Horcajada, C. Serre, M. Vallet-Regí, M. Sebban, F. Taulelle and G. Férey, *Angew. Chem. Int. Ed.,* 2006, **45**, 5974-5978; b) P. Horcajada, T. Chalati, C. Serre, B. Gillet, C. Sebrie, T. Baati, J. F. Eubank, D. Heurtaux, P. Clayette, C. Kreuz, J.-S. Chang, Y. K. Hwang, V. Marsaud, P.-N. Bories, L. Cynober, S. Gil, G. Férey, P. Couvreur and R. Gref, *Nat. Mater.,* 2010, **9**, 172-178; c) P. Horcajada, R. Gref, T. Baati, P. K. Allan, G. Maurin, P. Couvreur, G. Férey, R. E. Morris and C. Serre, *Chem. Rev.,* 2012, **112**, 1232-1268.

3. a) M. Yoon, R. Srirambalaji and K. Kim, *Chem. Rev.,* 2012, **112**, 1196-1231; b) J. Y. Lee, O. K. Farha, J. Roberts, K. A. Scheidt, S. T. Nguyen and J. T. Hupp, *Chem. Soc. Rev.,* 2009, **38**, 1450-1459; c) L. Ma, C. Abney and W. Lin, *Chem. Soc. Rev.,* 2009, **38**, 1248; d) M. A. El-Shall, V. Abdelsayed, A. E. R. S. Khder, H. M. A. Hassan, H. M. El-Kaderi and T. E. Reich, *J. Mater. Chem.,* 2009, **19**, 7625-7631.

4. a) T. K. Kim, J. H. Lee, D. Moon and H. R. Moon, *Inorg. Chem.,* 2013, **52**, 589-595; b) G. Liu, Y. Qin, L. Jing, G. Wei and H. Li, *Chem. Commun.,* 2013, **49**, 1699-1701; c) F.-Y. Yi, W. Yang and Z.-M. Sun, *J. Mater. Chem.,* 2012, **22**, 23201-23209; d) Y. W. Li, J. R. Li, L. F. Wang, B. Y. Zhou, Q. Chen and X. H. Bu, *J. Mater. Chem. A,* 2013, **1**, 495-499.

5. a) E. Y. Lee, S. Y. Jang and M. P. Suh, *J. Am. Chem. Soc.* 2005, **127**, 6374-6381; b) B. Chen, Y. Yang, F. Zapata, G. Lin, G. Qian and E. B. Lobkovsky, *Adv. Mater.,* 2007, **19**, 1693-1696; c) Z. Xie, L. Ma, K. E. deKrafft, A. Jin and W. Lin, *J. Am. Chem. Soc.,* 2010, **132**, 922-923; d) Y. Li, S. Zhang and D. Song, *Angew. Chem. Int. Ed.,* 2013, **52**, 710-713; e) B. V. Harbuzaru, A. Corma, F. Rey, J. L. Jordá, D. Ananias, L. D. Carlos and J. Rocha, *Angew. Chem. Int.*

Ed., 2009, **48**, 6476-6479; f) Y. Cui, H. Xu, Y. Yue, Z. Guo, J. Yu, Z. Chen, J. Gao, Y. Yang, G. Qian and B. Chen, *J. Am. Chem. Soc.,* 2012, **134**, 3979-3982.

6. Y. Cui, Y. Yue, G. Qian, B. Chen, *Chem. Rev.* 2012, ***112***, 1126-1162.
7. E. Kreno, K. Leorg, O. K. Farha, M. Allendorf, R. P. Van Duyne and J. T. Hupp, *Chem. Rev.,* 2012, **112**, 1105-1125.
8. a) Y. Salinas, R. Martínez-Máñez, M. D. Marcos, F. Sancenón, A. M. Costero, M. Parra and S. Gil, *Chem. Soc. Rev.,* 2012, **41**, 1261-1296; b) Z. Hu, B. J. Deibert and J. Li, *Chem. Soc. Rev.,* 2014, **43**, 5815-5840.
9. A. Lan, K. Li, H. Wu, D. H. Olson, T. J. Emge, W. Ki, M. Hong and J. Li, *Angew. Chem. Int. Ed.,* 2009, **48**, 2334-2338.
10. D. Ma, B. Li, X. Zhou, Q. Zhou, K. Liu, G. Zeng, G. Li, Z. Shi and S. Feng, *Chem. Commun.,* 2013, ***49***, 8964-8966.
11. a) G. M. Sheldrick, SHELXTL NT, Program for Solution and Refinement of Crystal Structures, Version 5.1, University of Göttingen, Göttingen, Germany, 1997; b) A. L. J. Spek, *Appl. Crystallogr.* 2003, **36**, 7-13; c) A. L. Spek, *PLATON, A Multipurpose Crystallographic Tool*, Utrecht University, Utrecht, The Netherlands, 2001.
12. J. H. Cavka, S. Jakobsen, U. Olsbye, N. Guillou, C. Lamberti, S. Bordiga and K. P. Lillerud, *J. Am. Chem. Soc.,* 2008, **130**, 13850-13851.
13. M. Kim and Seth M. Cohen, *CrystEngComm,* 2012, **14**, 4096-4104.
14. a) W. Morris, B. Volosskiy, S. Demir, F. Gándara, P. L. McGrier, H. Furukawa, D. Cascio, J. F. Stoddart and O. M. Yaghi, *Inorg. Chem.*, 2012, **51**, 6443-6445; b) Z. Wei, Z.-Y. Gu, R. K. Arvapally, Y.-P. Chen, R. N. McDougald, Jr., J. F. Ivy, A. A. Yakovenko, D. Feng, M. A. Omary and H.-C. Zhou, *J. Am. Chem. Soc.,* 2014, **136**, 8269-8276; c) D. Feng, H.-L. Jiang, Y.-P. Chen, Z.-Y. Gu, Z. Wei and H.-C. Zhou, *Inorg. Chem.,* 2013, **52**, 12661-12667; d) D. Feng, Z.-Y. Gu, J.-R. Li, H.-L. Jiang, Z. Wei and H.-C. Zhou, *Angew. Chem. Int. Ed.*, 2012, **51**, 10307-10310; e) M. Zhang, Y.-P. Chen, M. Bosch, T. Gentle III, K. Wang, D. Feng, Z. U. Wang and H.-C. Zhou, *Angew. Chem. Int. Ed.,* 2014, **53**, 815-818; f) J. E. Mondloch, W. Bury,D. Fairen-Jimenez,S. Kwon, E. J. DeMarco, M. H. Weston,A. A. Sarjeant,S. T. Nguyen,P. C. Stair,R. Q. Snurr,Omar K. Farha and J. T. Hupp *J. Am. Chem. Soc.*, 2013, **135**, 10294-10297; g) D. Feng, W.-C. Chung, Z. Wei, Z-Y. Gu, H.-L. Jiang, Y.-P. Chen, D. J. Darensbourg and H.-C. Zhou, *J. Am. Chem. Soc.,* 2013, **135**, 17105-17110; h) H.-L. Jiang, D. Feng, K. Wang, Z-Y. Gu, Z. Wei, Y.-P. Chen, H.-C. Zhou, *J. Am. Chem. Soc.* 2013, **135**, 13934-13938.
15. G. Horvath and K. Kawazoe, *J. Chem. Eng. Jpn.,* 1983, **16**, 470-475.
16. S. Pramanik, C. Zheng, X. Zhang, T. J. Emge and J. Li, *J. Am. Chem. Soc.,* 2011, **133**, 4153-4155.
17. a) K. C. Stylianou, R. Heck, S. Y. Chong, J. Bacsa, J. T. A. Jones, Y. Z. Khimyak, D. Bradshaw and M. J. Rosseinsky, *J. Am. Chem. Soc.*, 2010, **132**, 4119-4130; b) K. S. Asha, K. Bhattacharyya and S. Mandal, *J. Mater. Chem. C*, 2014, **2**, 10073-10081; c) Y.-S. Xue, Y. He, L. Zhou, F.-J. Chen, Y. Xu, H.-B. Du, X.-Z. You and B. Chen, *J. Mater. Chem. A*, 2013, **1**, 4525-4530.
18. a) X. Q. Song, W. S. Liu, W. Dou, Y. W. Wang, M. R. Zheng and Z. P. Zang, *Eur. J. Inorg. Chem.,* 2008, 1901-1912; b) J. C. Dai, X. T. Wu, Z. Y. Fu, C. P. Cui, S. M. Hu, W. X. Du, L. M. Wu, H. H. Zhang and R. O. Sun, *Inorg. Chem.,* 2002, **41**, 1391-1396; c) J. Fan, H. F. Zhu, T. A. Okamura, W. Y. Sun, W. X. Tang and N. Ueyama, *New J. Chem.,* 2003, **27**, 1409-1411.
19. Y. Q. Huang, B. Ding, H. B. Song, B. Zhao, P. Ren, P. Cheng, H. G. Wang, D. Z. Liao and S. P. Yan, *Chem. Commun.,* 2006, 4906-4908.
20. C. A. Bauer, T. V. Timofeeva, T. B. Settersten, B. D. Patterson, V. H. Liu, B. A. Simmons and M. D. Allendorf, *J. Am. Chem. Soc.,* 2007, **129**, 7136-7144.
21. M. Guo and Z.-M. Sun, *J. Mater. Chem.,* 2012, **22**, 15939-15946.
22. Q. Zheng, F. Yang, M. Deng, Y. Ling, X. Liu, Z. Chen, Y. Wang, L. Weng and Y. Zhou, *Inorg. Chem.,* 2013, **52**, 10368-10374.
23. J. Reungoat, J. S. Pic, M. H. Manéro and H. Debellefontaine, *Sep. Sci. Technol.*, 2007, **42**, 1447-1463.
24. a) H. Mangal, A. Saxena, A. S. Rawat, V. Kumar, P. K. Rai, M. Datta, *Micropor. Mesopor. Mater.* 2013, **168**, 247-256; b) S.-X. Liu, R. Wang, *J. Porous Mater.* 2011, **18**, 99-106.
25. a) M. Eddaoudi, J. Kim, N. Rosi, D. Vodak, J. Wachter, M. O'Keeffe and O. M. Yaghi, *Science,* 2002, 469-472; b) M. Eddaoudi, D. F. Sava, J. F. Eubank, K. Adil and V. Guillerm, *Chem. Soc. Rev.,* 2015, **44**, 228-249.
26. a) S. Hiroke, Y. Inubushi, T. Hori, T. Fukushima and S. Kitagawa, *Chem. Sci.,* 2012, **3**, 116-120; b) A. M. Avila, F. Yang, M. Shi and S. M. Kuznicki, *Chem. Eng. Sci.,* 2011, **66**, 2991-2996; c) N. B. K. Magnowski, A. M. Avila, C. C. H. Lin, M. Shi and S. M. Kuznicki, *Chem Eng Sci.,* 2011, **66**, 1697-1701; d) P. R. Pereira, J. Pires and M. B. de Carvalho, *Sep. Purif. Technol.,* 2001, **21**, 237-246; e) Y. He, Z. Zhang, S. Xiang, F. R. Fronczek, R. Krishna and B. Chen, *Chem. Eur J.,* 2012, **18**, 613-619; f) Y. He, Z. Zhang, S. Xiang, H. Wu, F. Fronczek, W. Zhou, R. Krishna, M. O'Keeffe and B. Chen, *Chem. Eur. J.,* 2012, **18**, 1901–1904.
27. a) B. Yuan, X. Wu, Y. Chen, J. Huang, H. Luo, S. Deng, *J. Colloid Interface Sci.* 2013, **394**, 445-450; b) M. C. Das, H. Xu, S. Xiang, Z. Zhang, H. D. Arman, G. Qian, B. Chen, *Chem. Eur. J.* 2011, **17**, 7817–7822.

Graphical Abstract

A Luminescent Zr-Based Metal-Organic Framework for Sensing/Capture of Nitrobenzene and High-Pressure Separation of CH_4/C_2H_6

Ruyi Zou, Xueling Ren, Fang Huang, Yifang Zhao, Jia Liu, Xiping Jing, Fuhui Liao, Yinxia Wang, Jianhua Lin, Ruqiang Zou, Junliang Sun

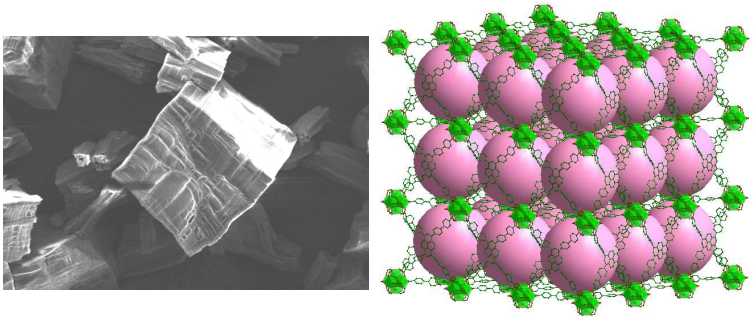

A novel LMOF based on a new tetracarboxylate ligand is reported with not only high performance of sensing and capture of nitrobenzene but also high-pressure separation of CH_4/C_2H_6.